Tunneling Spectroscopy of c-Axis $Y_{1-x}Ca_xBa_2Cu_3O_{7-\delta}$ Thin-Film Superconductors

J. H. Ngai,[1] W. A. Atkinson,[2] and J. Y. T. Wei[1]

[1]*Department of Physics, University of Toronto, Toronto, Ontario, M5S1A7 Canada*

[2]*Department of Physics and Astronomy, Trent University, Peterborough, Ontario K9J 7B8 Canada*

(Received 1 November 2006; published 25 April 2007)

Scanning tunneling spectroscopy was performed on c-axis $Y_{1-x}Ca_xBa_2Cu_3O_{7-\delta}$ thin films for $x = 0$, 0.05, 0.15, and 0.20 at 4.2 K. The measured spectra show main-gap, subgap, and satellite features which scale similarly in energy *versus* Ca doping, suggesting that they are associated with a single pairing energy. The data are analyzed with a multiband tunneling model which attributes the subgap features to the chain band and the satellite and main-gap features to the plane band for $d_{x^2-y^2} + s$ pairing symmetry. These results suggest that the superconductivity in $Y_{1-x}Ca_xBa_2Cu_3O_{7-\delta}$ involves multiple bands.

DOI: 10.1103/PhysRevLett.98.177003 PACS numbers: 74.72.Bk, 74.25.Jb, 74.50.+r, 74.62.Dh

Common to all the copper-oxide based high-temperature superconducting compounds are the CuO_2 planes. The CuO_2 planes are believed to be responsible for the wealth of phenomena observed in these materials [1], particularly the formation of Cooper pairs with $d_{x^2-y^2}$ symmetry [2]. $YBa_2Cu_3O_{7-\delta}$ (YBCO) is peculiar among the cuprates in that it also has quasi-one-dimensional, metallic CuO chains, which may contain finite superfluid density below the superconducting critical temperature (T_c) as suggested by various bulk probes [3–5]. Since long-range order cannot be easily sustained in one dimension, the apparent presence of superfluid density in the chains suggests that the plane and chain bands are electronically coupled. Such coupling would imply that the superconductivity in YBCO is essentially multiband in nature [6–11], and could conceivably affect its pairing symmetry. In fact, recent pair-tunneling experiments [12,13] have revealed a twofold, $d_{x^2-y^2} + s$ pairing symmetry [14,15] in optimally doped YBCO, with the d-wave node lines rotated away from the chain axis.

At present it is not yet clear from these pair-tunneling experiments whether the observed $d + s$ pairing symmetry is intrinsic to the planes [16] or if it is an effect of coupling between the plane and chain bands [6–10]. Quasiparticle tunneling spectroscopy could help to elucidate this issue by revealing multigap features in the excitation spectrum and by providing information about the pairing symmetry. For example, quasiparticle tunneling experiments on MgB_2 have revealed multiple s-wave gaps arising from multiband coupling [17,18]. In the case of YBCO, c-axis tunneling spectroscopy experiments have revealed multiple spectral features in addition to the predominant d-wave gap [19–22]. It would be important to understand the origin of these additional spectral features. Furthermore, since both multiband coupling in general [23] and pairing symmetry in the cuprates may vary with carrier doping [24], a detailed study of the spectral evolution with doping could yield crucial insights on the pairing in YBCO.

In this Letter, we present a scanning tunneling spectroscopy (STS) study of Ca-doped c-axis YBCO films at 4.2 K. The measured spectra show main-gap, subgap, and satellite features which scale similarly in energy as a function of Ca doping, suggesting that they are associated with a single pairing energy. The data are analyzed with a generic tunneling model which indicates that the main-gap and subgap features can be associated with the plane and chain bands, respectively, while the satellite feature can be attributed to $d + s$ splitting of the gap maximum in the plane band. These results suggest that the superconductivity in YBCO involves both the plane and chain bands.

The $Y_{1-x}Ca_xBa_2Cu_3O_{7-\delta}$ thin films measured were epitaxially grown by pulsed laser-ablated deposition (PLD) to ~50 nm thickness on (100)-oriented $SrTiO_3$ substrates. The films were made from targets with nominal $x = 0$, 0.05, 0.15, 0.20 Ca-doping concentrations. Two to three films were made for each doping concentration resulting in average measured T_c values of 89 K, 85 K, 81 K, and 78 K, respectively. Cation substitution of Ca^{2+} for Y^{3+} in the unit cell is known to introduce additional holes into the CuO_2 planes, thus overdoping the films and lowering the T_c [25]. The films were transferred from the PLD chamber to the STS apparatus with less than 10 minutes exposure to air. STS was performed at 4.2 K with either chemically etched or mechanically sheared Pt-Ir tips by measuring the tunneling current I versus the sample bias voltage V. The measured I-V spectra were numerically differentiated to obtain the conductance dI/dV spectra.

Figure 1 shows representative dI/dV spectra taken at 4.2 K on an optimally doped ($x = 0$) c-axis film. The spectra, staggered for clarity, were taken every 3 nm over the film surface, demonstrating good spatial homogeneity. A robust main-gap feature is observed along with a weaker above-gap, satellite feature indicated by arrows in the bottom spectrum of Fig. 1. A weak subgap feature is also visible, becoming more pronounced with Ca doping as will be discussed below. All three spectral features have often been seen in previous c-axis tunneling experiments on YBCO single crystals and thin films, with both planar-junction and STS geometries [19–22,26].

Figure 2 shows two types of spectra measured on different locations over a $x = 0.05$ Ca-doped film. Both spectral

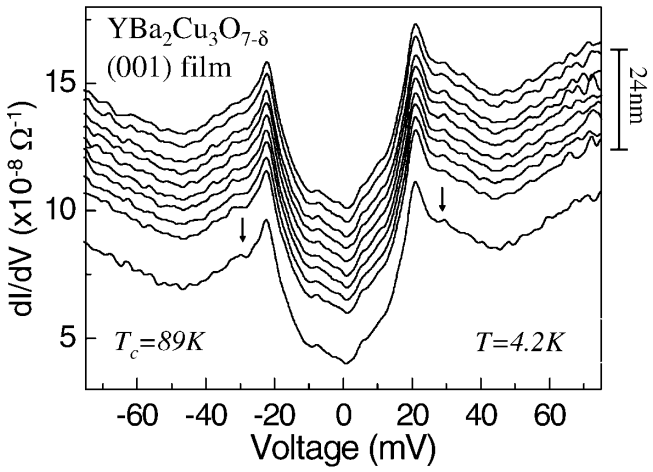

FIG. 1. Representative tunneling spectra taken on an optimally doped c-axis $YBa_2Cu_3O_{7-\delta}$ thin film at 4.2 K. The spectra shown (staggered for clarity) were taken 3 nm apart. Outer arrows indicate the satellite features.

types exhibit the main-gap peaks, as well as the satellite features, while the spectrum in Fig. 2(b) also exhibits pronounced subgap features, as indicated by the arrows inside the main gap. We also note that the main-gap peak heights are more pronounced in Fig. 2(a) than in Fig. 2(b). In general, all the Ca-doped YBCO thin films show spectral variations beyond length scales of $\sim$20 nm. This inhomogeneity was also observed in previous STS studies of similar Ca-doped YBCO thin films, indicating that this may be an effect of Ca substitution [27,28]. Despite this spectral variation, the same generic features were consistently seen in our films up to $x = 0.15$. The main panel of Fig. 3 plots data for a $x = 0.15$ film, again showing the main-gap, subgap, and satellite features, indicating their prevalence in Ca-doped YBCO.

Figure 4 shows the evolution of these spectral features with Ca doping. Assuming these features correspond to gap energies, a general trend of decreasing gap size versus increasing doping is observed. Quite remarkably, these spectral features show similar scaling in energy as a function of doping, as indicated by the roughly constant ratios of either satellite to main-gap or subgap to main-gap values in the inset of Fig. 4. While there are several scenarios that could lead to multiple peaks in the tunneling spectrum [9,29], this apparent energy scaling suggests that there is a *single* pairing energy responsible for all three spectral features. This pairing energy presumably corresponds to the predominant pairing interaction in the CuO_2 planes.

In order to understand how multiple spectral features could arise from a single pairing energy in YBCO, we discuss a multiband scenario in which the CuO chain band is coupled to the CuO_2 plane band with an overall $d_{x^2-y^2} + s$ pairing symmetry. First, if one characterizes the order parameter in the plane by $\Delta_p(k) = \Delta_0[\cos(k_x) - \cos(k_y)]/2 + \Delta_s$ with the ratio $\Delta_s/\Delta_0 \approx 0.15$ [12,13],

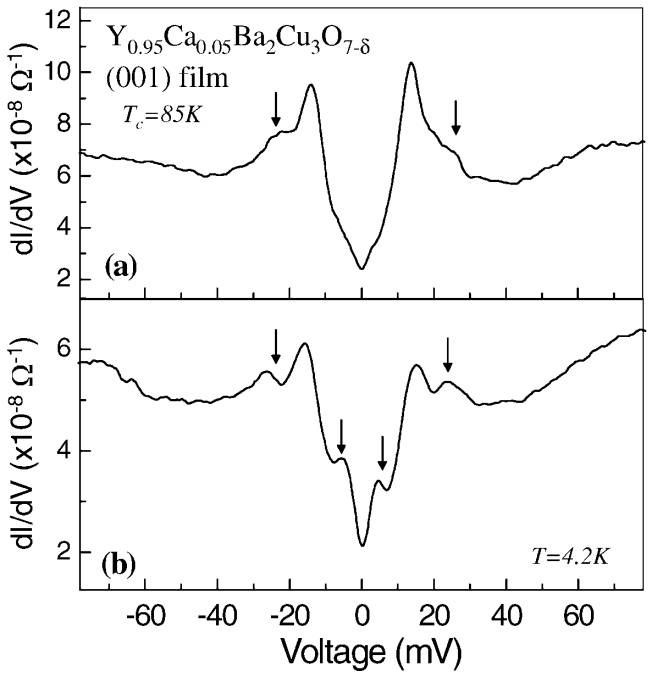

FIG. 2. Representative tunneling spectra taken on a c-axis $Y_{0.95}Ca_{0.05}Ba_2Cu_3O_{7-\delta}$ thin film at 4.2 K. Both (a) and (b) were taken on different spots on the same film, showing some spectral variation but the same generic features and similar main-gap sizes. Inner and outer arrows indicate the subgap and satellite features, respectively.

then the d-wave gap peak splits into main and satellite peaks [8]. Second, in chain-plane coupling scenarios with the pairing interaction being predominantly in the plane, the gap function in the chain $\Delta_c(k)$ is proportional to $\Delta_p(k)$, creating a subgap energy scale [8–10]. We illustrate

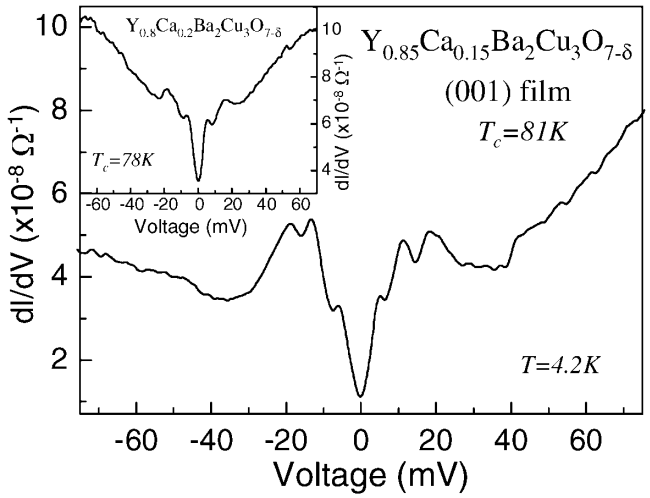

FIG. 3. Representative tunneling spectrum taken on a c-axis $Y_{0.85}Ca_{0.15}Ba_2Cu_3O_{7-\delta}$ thin film at 4.2 K. (inset) Tunneling spectrum taken on a c-axis $Y_{0.80}Ca_{0.20}Ba_2Cu_3O_{7-\delta}$ thin film at 4.2 K showing one of the larger main-gaps measured.

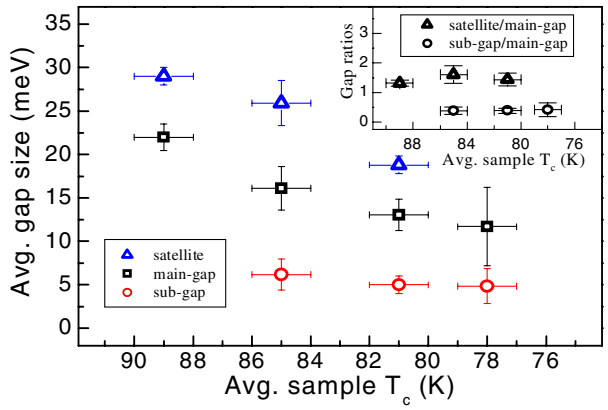

FIG. 4 (color online). Average gap sizes, corresponding to the satellite (△), main-gap (□), and subgap (○) features, plotted as a function of the average sample T_c. Inset shows the average gap ratios, between satellite to main-gap (△) and subgap to main-gap values (○).

these points with a generic tunneling model consisting of a two-dimensional plane band and a one-dimensional chain band without explicit account of their coupling. In this simplified model, the normal-state plane dispersion is

$$\xi_p(k) = -2t_1\{\cos(k_x) + \cos(k_y) + 2t' \cos(k_x)\cos(k_y) + t''[\cos(2k_x) + \cos(2k_y)]\} - \mu_1, \quad (1)$$

where $t' = -0.1$, $t'' = 0.25$, and $\mu_1 = \mu - \epsilon_1$, where μ is the chemical potential and ϵ_1 a constant potential associated with the planes. We describe the normal-state chain dispersion by

$$\xi_c = -2t_2 \cos(k_y) - \mu_2, \quad (2)$$

where $\mu_2 = \mu - \epsilon_2$, and where the potential difference $\epsilon_2 - \epsilon_1$ determines the relative offset between the bottoms of the plane and chain bands. The parameters t_1, t_2 represent the nearest-neighbor overlap integrals in the plane and chain bands, respectively. We calculate the superconducting dispersion for each band via the BCS relation $E^2_{p,c}(k) = \xi^2_{p,c}(k) + \Delta^2_{p,c}(k)$, where for the chain gap function we take the simplest possible ansatz $\Delta_c(k) = \Delta_p(k)$, which allows us to illustrate our model. In reality, the induced gap in the chains will have a more complicated structure [9]. However, our model presented here is sufficient to capture many of the essential features predicted by a more thorough treatment, which calculates the coupling between the plane and chain layers explicitly [29].

We use the following parameter values $\{t_1, t_2, \mu_1, \mu_2\} = \{120, 300, -86, -350\}$ meV to calculate the Fermi surfaces of the plane (red) and chain (orange) bands shown in Fig. 5(a). Following the c-axis quasiparticle tunneling formalism described in Ref. [30], we calculate the dI/dV spectra for the plane (solid line) and chain (dashed line) bands using the $d + s$ gap function introduced above and show the results in Fig. 5(c). For comparison, we show the

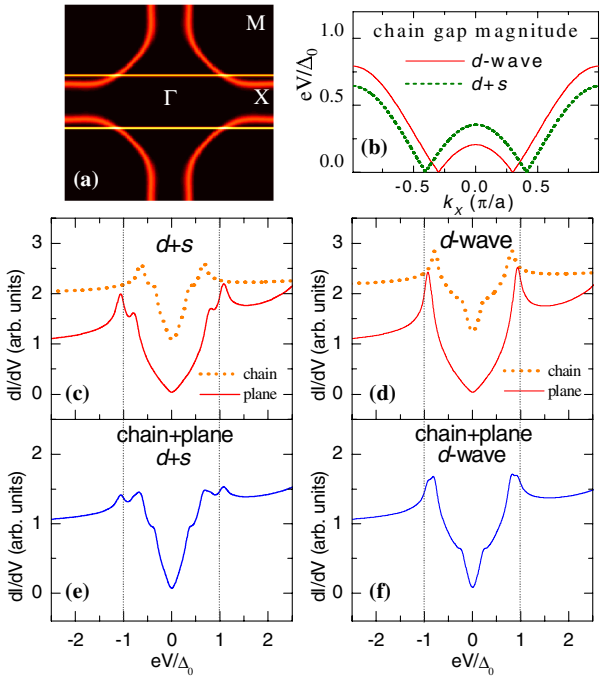

FIG. 5 (color online). Two-band quasiparticle tunneling model used to describe the main-gap, subgap, and satellite features. (a) Fermi surface used in our model with the 2D plane band shown in red and the 1D chain band shown in orange. (b) Amplitudes of the d-wave and $d + s$ gap functions projected on to the chain Fermi surface while moving along k_x. (c) Calculated $d + s$ spectra for the plane band (solid line) and chain band (dashed line). (d) Calculated d-wave spectra for the plane band (solid line) and chain band (dashed line). (e) Combined plane and chain spectrum for $d + s$ scenario. (f) Combined plane and chain spectrum for pure d-wave scenario.

calculated spectra for a pure d-wave gap function in Fig. 5(d). Because of the anisotropic nature of both the gap function and the band dispersions, the Fermi surface does not generally intersect with k-space regions where the gap function is maximum. Figure 5(b) illustrates this scenario for the chain band, showing the d-wave and $d + s$ gap function amplitudes projected onto the chain Fermi surface along k_x. For the plane band, a similar scenario occurs. As a result of this *band structure enhanced* gap anisotropy, the k-space averaged value of the gap edge measured by quasiparticle tunneling will tend to be smaller than Δ_0. This tendency is shown in Fig. 5(c)–5(f), where Δ_0 is indicated by the dotted vertical lines. At present, our knowledge of the tunneling matrix elements between the tip and the individual plane and chain bands is incomplete [30]. Therefore, the relative weighting of each band in a given tunnel junction is unknown. To illustrate a multiband situation, we assume a 30% plane to 70% chain band weighting and plot a combined spectrum in Fig. 5(e) and 5(f) [17,18,21]. For the parameters used above, the $d + s$ gap function produces three spectral features, while only two are produced for the d-wave gap function. In compar-

ing Fig. 5(e) with Fig. 3, it is clear that the spectral features seen in our data can be attributed to a multiband scenario with $d + s$ pairing symmetry.

On the premise that these spectral features arise from the plane and chain bands, a few remarks should be made on the origin of the $d + s$ pairing symmetry, and on the doping evolution of both the s-wave component and the chain-plane coupling. First, O'Donovan and Carbotte [8] have shown that the self-consistently solved order-parameter pairing symmetry in a coupled plane and chain system is $d + s$. The predictions of their calculation are consistent with our experimental observations, and could explain the origin of the s-wave component in YBCO.

Second, the 15% s-wave component as reported in pair-tunneling experiments [12,13] is within the error bars of our data up to $x = 0.15$ Ca doping. Beyond this doping level, the satellite feature is not discernible, as evidenced by the inset of Fig. 3, showing one of the larger main-gaps observed on a $x = 0.20$ film. Thus, at present we cannot tell if the satellite feature has merged with the main-gap peak or if the former has weakened to become indistinguishable from the spectral background. The scenario of the satellite and main peak merging would suggest that the s-wave component has disappeared at the higher doping, leaving behind a purely d-wave pairing symmetry [Fig. 5(f)]. Further studies using other experimental techniques would be necessary to elucidate this issue.

Third, our data indicate that as YBCO is Ca doped, the main-gap peaks are suppressed while the subgap features become more pronounced, suggesting that the chain-plane coupling could be changing with doping. This observation may be consistent with recent Raman scattering data showing an increase in the chain-plane coupling with Ca doping [24]. Although our simple multiband tunneling model can explain the multiple spectral features we observed, a more rigorous theoretical treatment of the chain and plane coupling would be necessary to describe the peak-height evolution with doping [9].

Lastly, we note that tunneling studies of (110)-oriented Ca-doped YBCO thin films have observed a split zero-bias conductance peak (ZBCP) structure, which resembles the subgap features we observed on c-axis thin films [28]. However, the ZBCP splitting was observed to increase with Ca doping [28], in contrast to how the subgap feature evolves in our c-axis data. This difference clearly distinguishes the two junction orientations as probing different phenomena [22].

In summary, we have performed scanning tunneling spectroscopy measurements on c-axis $Y_{1-x}Ca_xBa_2Cu_3O_{7-\delta}$ thin films at 4.2 K to study the evolution of the main-gap, subgap, and satellite features with Ca doping. These spectral features scale similarly in energy as a function of doping, suggesting that they are associated with a single pairing energy. Using a multiband tunneling model, our analysis indicates that the subgap and main-gap features can be attributed to the chain and plane bands, respectively, while the satellite feature could arise from $d + s$ splitting of the gap maximum in the plane band. These results suggest that the superconductivity in $Y_{1-x}Ca_xBa_2Cu_3O_{7-\delta}$ involves multiple bands.

This work was supported by grants from NSERC, CFI, OIT, MMO/EMK, and the Canadian Institute for Advanced Research in the Quantum Materials Program. J. H. N. would like to thank the WCS Foundation for funding.

[1] J. Orenstein and A. J. Millis, Science **288**, 468 (2000).
[2] C. C. Tsuei and J. R. Kirtley, Rev. Mod. Phys. **72**, 969 (2000); D. J. van Harlingen, *ibid.* **67**, 515 (1995).
[3] D. N. Basov *et al.*, Phys. Rev. Lett. **74**, 598 (1995).
[4] W. N. Hardy *et al.*, Phys. Rev. Lett. **70**, 3999 (1993).
[5] R. Gagnon *et al.*, Phys. Rev. Lett. **78**, 1976 (1997).
[6] M. Tachiki *et al.*, Z. Phys. B **80**, 161 (1990).
[7] I. I. Mazin *et al.*, Physica C (Amsterdam) **209**, 125 (1993).
[8] C. O'Donovan and J. P. Carbotte, Phys. Rev. B **55**, 1200 (1997).
[9] W. A. Atkinson, Phys. Rev. B **59**, 3377 (1999).
[10] D. K. Morr and A. V. Balatsky, Phys. Rev. Lett. **87**, 247002 (2001).
[11] H. L. Edwards *et al.*, Phys. Rev. Lett. **75**, 1387 (1995).
[12] H. J. H. Smilde *et al.*, Phys. Rev. Lett. **95**, 257001 (2005).
[13] J. R. Kirtley *et al.*, Nature Phys. **2**, 190 (2006).
[14] A. G. Sun *et al.*, Phys. Rev. Lett. **72**, 2267 (1994).
[15] K. A. Kouznetsov *et al.*, Phys. Rev. Lett. **79**, 3050 (1997).
[16] D. H. Lu *et al.*, Phys. Rev. Lett. **86**, 4370 (2001).
[17] H. Schmidt *et al.*, Phys. Rev. Lett. **88**, 127002 (2002).
[18] M. Iavarone *et al.*, Phys. Rev. Lett. **89**, 187002 (2002).
[19] J. M. Valles *et al.*, Phys. Rev. B **44**, 11 986 (1991).
[20] I. Maggio-Aprile *et al.*, Phys. Rev. Lett. **75**, 2754 (1995).
[21] A. M. Cucolo *et al.*, Phys. Rev. B **46**, 5864 (1992).
[22] J. Y. T. Wei *et al.*, Phys. Rev. Lett. **81**, 2542 (1998).
[23] G. Binnig *et al.*, Phys. Rev. Lett. **45**, 1352 (1980).
[24] T. Masui *et al.*, Phys. Rev. B **68**, 060506 (2003); Phys. Rev. Lett. **95**, 207001 (2005).
[25] G. Böttger *et al.*, J. Phys. Condens. Matter **8**, 8889 (1996).
[26] J. Ngai *et al.*, Phys. Rev. B **72**, 054513 (2005).
[27] N.-C. Yeh *et al.*, Phys. Rev. Lett. **87**, 087003 (2001).
[28] G. Deutscher, Rev. Mod. Phys. **77**, 109 (2005) and references therein.
[29] W. A. Atkinson (to be published).
[30] J. Y. T. Wei *et al.*, Phys. Rev. B **57**, 3650 (1998); B. W. Hoogenboom *et al.*, Phys. Rev. B **67**, 224502 (2003).